Interlayer Mass Transport in Homoepitaxial and Heteroepitaxial Metal Growth

Karsten Bromann, Harald Brune, Holger Röder, and Klaus Kern
Institut de Physique Expérimentale, Ecole Polytechnique Fédérale-Lausanne, CH-1015 Lausanne, Switzerland
(Received 13 March 1995)

We describe a general method for the quantitative determination of the interlayer mass transport in epitaxial growth. Through measurement of the nucleation rate on top of islands as a function of island size and temperature, the additional barrier for an adatom to descend the step edge ΔE_s can be determined with high accuracy. This approach is applied to the growth of Ag on the (111) surfaces of Ag and Pt. In the homoepitaxial system, the barrier is found to be $\Delta E_s = 120 \pm 15$ meV, whereas in the heteroepitaxial case it is substantially lowered, $\Delta E_s = 30 \pm 5$ meV.

PACS numbers: 68.55.–a, 61.16.Ch, 68.35.Bs

The ultimate goal in epitaxial growth is the controlled fabrication of atomically thin films with smooth abrupt interfaces. In the thermodynamic limit, the growth morphology is determined by the balance of the interfacial energies involved [1]. In most cases, thin films are grown under experimental conditions far from equilibrium. Film growth and the resulting morphology will then be governed by kinetic effects. If the interlayer mass transport is sufficiently fast to allow atoms to leave the tops of growing two-dimensional islands as fast as they arrive, the growing layer will be completed before second-layer nucleation sets in and smooth layer-by-layer growth results. This is in general a delicate balance between several factors like the deposition rate, the density, size, and shape of adlayer islands, the adatom diffusion barrier, and finally the activation barrier for an adatom to descend at the edges of adatom islands. The step-edge barrier E_s accounts for the fact that the diffusion barrier of an adatom over the edge of a step is different from that on the terrace [2,3]. Usually it is harder to step down from an upper terrace than to remain on the same level, i.e., $E_s > E_d$, with E_d the barrier of terrace diffusion.

Many microscopic details of the growth kinetics have recently been revealed by studies of Ag and Pt homoepitaxy on their (111) surfaces [4–8]. Here, kinetic effects could be studied in their pure form, as structural misfits and electronic inhomogeneities are absent. Both systems were found to grow in a multilayer (3D) growth mode at 300 K which was attributed to the limited interlayer mass transport at this temperature, ascribed to relatively large barrier heights for an adatom to descend a step edge. While the lateral diffusion barrier E_d governing the intralayer mass transport has been quantitatively determined for numerous metal systems [9,10], quantitative measurements of the step-edge barrier E_s, though first postulated nearly 30 years ago, are rare [11,12].

In this Letter we present a general method for the quantitative determination of the interlayer mass transport in epitaxial growth. The method is based on the measurement of the nucleation rate on top of previously grown adlayer islands as a function of island size and temperature. The additional step-edge barrier $\Delta E_s = E_s - E_d$, i.e., the barrier for an adatom to descend the step edge minus the surface diffusion barrier, as well as the corresponding attempt frequency ν_s can be determined with high accuracy. This approach is applied to Ag homoepitaxy and heteroepitaxy on the (111) surfaces of Ag and Pt. In the homoepitaxial system, the additional step-edge barrier is found to be $\Delta E_s = 120$ meV. In the heteroepitaxial case, ΔE_s is substantially lowered to $\Delta E_s = 30$ meV. This dramatic decrease of the step-edge barrier is likely to be associated with the preferential strain relief at the edges of heteroepitaxial islands facilitating the descent of an adatom.

Figure 1 illustrates the method. Two-dimensional adlayer islands of well-defined size are built via evaporation of a submonolayer coverage at low temperatures and subsequent annealing [Figs. 1(a) and 1(b)], as described in detail in Ref. [13]. After a second evaporation of a submonolayer coverage, the nucleation on top of the preexistent islands and its dependence on the island size and temperature is examined [Figs. 1(c)–1(f)]. The quantitative description of the experiment is based on nucleation theory and follows the idea of a critical island size for layer-by-layer growth [7]. In the absence of stable clusters, the adatom density on top of a compact island of radius R is a function of the distance from the island center and obeys the diffusion equation. Under steady-state conditions, the incident atom flux onto an island equals the step-down diffusion from the island at its perimeter. The coefficient for step-down diffusion $S = C_s \nu_s \exp[-E_s/kT]$, C_s being a symmetry factor of order unity, enters thus via the boundary condition for the adatom density on top of an island. Knowing the spatial dependence of this adatom density, one can calculate the rate Ω at which a stable cluster nucleates on top of an island of radius R by integrating the local nucleation rate over the area of the island. This leads to Eq. (3) of Ref. [7] which reads

$$\Omega = \frac{\pi \gamma D}{i+2}\left(\frac{F}{4D}\right)^{i+1} a^{2i-2}\left[\left(R^2 + \frac{2a}{\alpha}R\right)^{i+2} - \left(\frac{2a}{\alpha}R\right)^{i+2}\right]. \quad (1)$$

Here, F is the incident atom flux, $D = C_d a^2 \nu_d \exp[-E_d/kT]$ (C_d being a symmetry factor

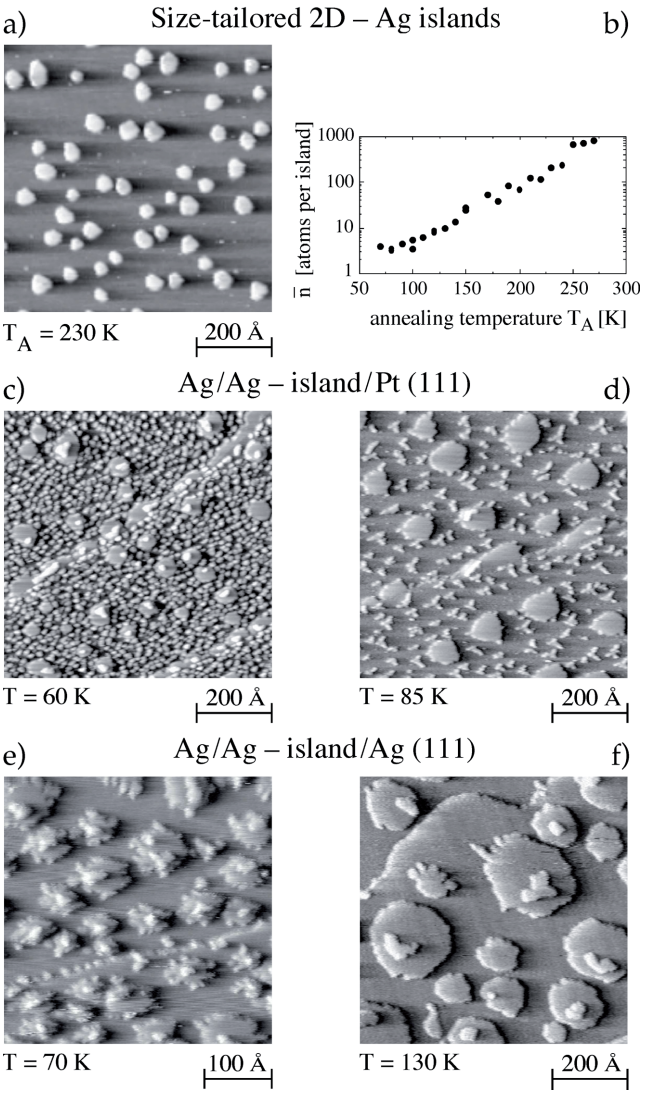

FIG. 1. The STM image (a) and the graph (b) illustrate the building of 2D Ag islands on Pt(111) with defined sizes via deposition of 0.1 ML silver at 40 K and subsequent annealing. In (a) the annealing temperature was 230 K. The STM images (c)–(f) show the subsequent growth step in which 0.1 ML Ag are deposited (flux = 1.1×10^{-3} ML/s) on the previously grown islands. In (c) and (d), Ag is evaporated onto Ag islands on Pt(111) at temperatures of 60 K (c) and 85 K (d), respectively. In (e) and (f), Ag is evaporated onto Ag islands on Ag(111) at temperatures of 70 K (d) and 130 K (f), respectively. The STM images are measured isothermally at the temperatures of the second evaporation step. All images are taken in differential mode, which means that the derivative of the lines of constant tunnel current is recorded.

similar to C_s) is the terrace diffusion coefficient, a^2 is the area of the surface unit cell, and i denotes the size of the critical cluster. For $i = 1$, γ is of order unity. $\alpha = a^2 S/D = (\nu_s/\nu_d)\exp[-\Delta E_s/kT]$ is the quotient of the coefficients for step-down and terrace diffusion.

The fraction f of islands on which a stable cluster has nucleated increases during the second evaporation as $df/dt = \Omega(1 - f)$, which leads to

$$f = 1 - \exp\left[-\int_t \Omega(R)\, dt\right]. \tag{2}$$

The integral describes the growth of the preexistent islands during evaporation time t and has to be treated differently for two limiting cases: (i) All of the material impinging during the second evaporation causes an increase in the size of the previously grown islands. No nucleation occurs between the islands [realized for Ag/Ag(111), see Figs. 1(e) and 1(f)]. (ii) The mean diffusion length of the adatoms during the second evaporation is much smaller than the distances between the preexistent islands. Nucleation occurs on the terrace, and only the material that lands on top of an island causes its growth [realized for Ag/Ag/Pt(111), see Figs. 1(c) and 1(d)]. Hence, for the cases (i) and (ii), the increase of the island radius R of an island during the second evaporation has to be described differently. Knowing the coverage of both evaporations and the density of the preexistent islands, one can directly calculate the fraction of covered islands as a function of island radius R after the second evaporation.

Equation (2) predicts that the probability of finding second monolayer nucleation on top of the previously grown islands will rapidly change from nearly 0 for small islands to nearly 1 for large ones. The critical radius R at which this transition takes place depends strongly on temperature, as Ω is a function of α which varies as $\exp[-\Delta E_s/kT]$. One can thus separate the influence of the attempt frequencies ν_s/ν_d from the additional activation barrier ΔE_s by measurements at various temperatures.

We applied this method to Ag/Ag(111) homoepitaxy and Ag/Pt(111) heteroepitaxy. The experiments were performed with a variable temperature scanning tunneling microscope (STM) mounted in UHV which operates in the temperature range from 25 to 800 K [14]. The Pt(111) crystal was cleaned by repeated cycles of Ar ion sputtering (750 eV) at 800 K and subsequent annealing at 1200 K. The Ag(111) surface was prepared by epitaxial growth of 50 monolayer (ML) thick Ag films on the Pt(111) surface [15]. The Ag submonolayers were evaporated with a Knudsen cell at a background pressure better than 2×10^{-10} mbar. The 2D Ag islands were grown by evaporation of 0.1 ML Ag at 40 K and subsequent annealing. This yields a population of compact 2D islands with a relatively sharp size distribution [Figs. 1(a) and 1(b), see Ref. [13] for details]. For the present study we have tailored islands of average radii ranging from 10 to 100 Å. This size range assures that ΔE_s is independent of the island size. Only for small clusters with less than about 50 atoms (i.e., typical radii <10 Å) has the additional step-edge barrier theoretically been found to be size dependent [16].

The STM data in Fig. 1 show the expected behavior. At low temperatures, the onset of second monolayer growth

takes place on many of the relatively small islands, whereas at higher temperatures the tops of even much bigger islands are devoid of nucleated clusters [Figs. 1(c)–1(f)]. In Fig. 2, the experimental data are compared with the theoretical predictions of Eq. (2). The island radii have been corrected for the increased imaging width due to the finite curvature of the scanning tip. The values of the attempt frequencies and activation barriers for terrace diffusion, ν_d and E_d, and the size of the critical cluster i were determined independently by measurements of the saturation island density as a function of temperature for both systems, Ag/Ag(111) ($E_d = 97$ meV, $\nu_d = 2 \times 10^{11}$ s^{-1}, $i = 1$ for $T < 150$ K) and Ag/1 ML Ag/Pt(111) ($E_d = 60$ meV, $\nu_d = 1 \times 10^9$ s^{-1}, $i = 1$ for $T < 90$ K) [17]. Hence, the attempt frequency ν_s and the additional step-down activation energy ΔE_s are the only free parameters in the fits. It is important to note that the data for one single temperature can always by described by various combinations of ν_s and ΔE_s. The measurement of the temperature dependence of the step-down diffusion coefficient, however, allows one to distinguish between the influence of the attempt frequency and the activation barrier. The values obtained from the fits in Fig. 2 are $\Delta E_s = 120 \pm 15$ meV and $\nu_s = 1 \times 10^{(13\pm1)}$ s^{-1} for the system Ag/Ag islands/Ag(111) and $\Delta E_s = 30 \pm 5$ meV and $\nu_s = 1 \times 10^{(9\pm1)}$ s^{-1} for the system Ag/Ag islands/Pt(111). The experimental error is mainly caused by the inaccuracy of the island radii which can be determined with a precision of about 5 Å.

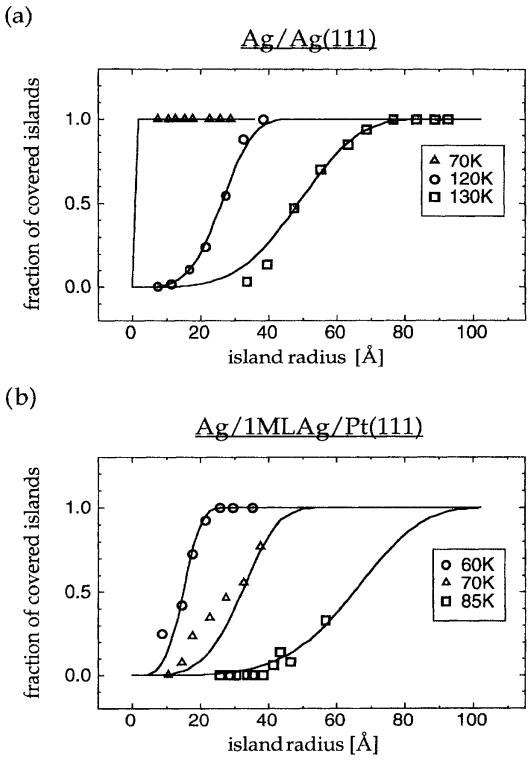

FIG. 2. Quantitative evaluation of the nucleation probability for Ag on 2D Ag islands on Ag(111) (a) and Pt(111) (b). The fraction of covered islands is shown as a function of island radius and deposition temperature (flux = 1.1×10^{-3} ML/s).

The step-edge barriers as determined in our experiment have to be interpreted as effective ones, resulting from the different pathways an adatom can use to descend. Theoretical studies show that the activation energy of interlayer diffusion on fcc (111) metal surfaces depends strongly on the atomic processes involved [16,18–20]. For these surfaces, exchange processes are energetically preferred with respect to direct hopping over the step edge, which has also been confirmed by field ion microscopy studies of the Ir(111) surface [21]. The theoretical studies reveal that, in particular, close to kink sites at the B-type steps, the lower atoms can easily be pulled outside, facilitating this exchange mechanism. Hence, at low temperatures, only those of the possible atomic processes with the lowest barrier should be thermally activated. As the size-tailored 2D islands in our experiment have a relatively high density of kinks (as evidenced by the fuzzy STM imaging of the island perimeters), the measured step-down activation barriers are likely to correspond to the kinetically favored exchange processes at kink sites. For this process Li and DePristo [16] calculated an additional step-edge barrier of only 50 meV for the homoepitaxial Ag(111) system, which is about a factor of 2 below our experimental value. This difference is, however, not too surprising as embedded atom and effective medium calculations usually underestimate diffusion barriers due to the incomplete account of the coordination at surfaces. In a very recent analysis of the occupancy of open layers as a function of coverage, developed for homoepitaxy, Meyer *et al.* found $\Delta E_s = 150 \pm 20$ meV for a Ag/Ag(111) from experiments at 300 K [8,22], which is in fair agreement with our measurement.

The step-down activation energy in the heteroepitaxial system Ag/Ag islands/Pt(111) is drastically lowered. This barrier of only 30 meV can easily be overcome, which is the reason for the perfect wetting of the first Ag monolayer on Pt(111) down to temperatures as low as 80 K. In this system, the Ag islands in the first monolayer grow pseudomorphically on the substrate and are thus under a substantial compressive strain of 4.2% [23]. The pseudomorphic islands preferentially relieve their strain at the edges where the Ag atoms are free to expand laterally. A second major difference to the homoepitaxial case is the different binding energy for an Ag adatom on the Pt(111) surface. While in homoepitaxy both upper and lower terraces are energetically on the same level, in the case of Ag/Pt(111) the upper Ag terrace is about 170 meV higher in energy than the lower Pt terrace [24] (see Fig. 3). Both effects may bend the step potential close to the step edge accounting for the substantial decrease in the step-edge barrier. It is difficult to decide *a priori* which of the two, the strain relief at edges or the electronic adlayer-substrate coupling, is the dominating effect. We have, however, recently studied quantitatively the influence of

lattice strain and electronic adlayer-substrate coupling for the Ag/Pt(111) system by effective medium calculations [17]. In these calculations, strain effects clearly dominate the electronic adlayer-substrate coupling. It is thus most likely that the preferential strain relief at the edges of the pseudomorphic Ag islands is the origin of the dramatic lowering of the step-edge barrier.

For the homoepitaxial Ag/Ag(111) system, the additional step-edge barrier is found to be comparable to the lateral adatom diffusion barrier, which explains the rough growth morphology experimentally observed below 400 K [5]. This seems to be a general trend for homoepitaxial growth on fcc (111) metal surfaces where ΔE_s has always been calculated to be of the same order as E_d [16,18–20]. Without affecting the intralayer diffusion, smooth growth morphologies at low temperatures can thus only be obtained via enhancement of the interlayer mass transport. This can be done either by increasing the visiting frequency of the adatoms at the step edge or by lowering the step-edge barrier. The latter has been demonstrated by Esch *et al.* [4(b)] to be effective in the oxygen-mediated layer-by-layer growth of Pt/Pt(111). The reduction of the barrier height for the motion of Pt adatoms across oxygen-covered step edges can be understood in light of the drastic barrier lowering for the compressively strained Ag islands on Pt(111). Pt islands on Pt(111) are under tensile stress. Chemisorption of an electronegative adsorbate (like oxygen) at the island edge weakens the bond between the core and the edge atoms of the Pt island accompanied by an outward relaxation of the edge atoms [25]. This lateral expansion at the edges of the islands should facilitate exchange diffusion processes and correspondingly lower their barriers. The specific lowering of the step-edge barrier via step decoration with electronegative surfactants should be a general phenomenon, which might be applied to grow smooth homoepitaxial and heteroepitaxial metal films at low temperatures.

In conclusion, we have described an experimental method for the quantitative determination of the effective activation barrier of interlayer mass transport in epitaxial growth. The concept is based on nucleation theory and uses variable temperature STM. We have determined the effective additional activation barriers as well as the corresponding attempt frequencies for step-down diffusion in Ag homoepitaxy and heteroepitaxy on the (111) surfaces of Ag and Pt. On the pseudomorphic Ag islands on Pt(111), the step-edge barrier is found to be substantially lowered with respect to the homoepitaxial system. This lowering is related to relaxation effects at the edges of the compressively strained islands. It is suggested that the lowering of the potential barrier observed for the descent of a Pt adatom across an oxygen-covered Pt step has the same microscopic origin.

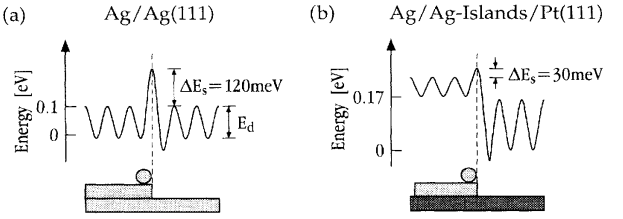

FIG. 3. Potential energy diagram characterizing the interlayer and intralayer diffusion in Ag homoepitaxy (a) and heteroepitaxy (b) at the (111) surfaces of Ag and Pt. The intralayer diffusion barriers are from Refs. [15] and [23], the difference in binding energy in case (b) from Ref. [22].

[1] E. Bauer, Z. Kristallogr. **110**, 423 (1958).
[2] R. L. Schwoebel and E. J. Shipsey, J. Appl. Phys. **37**, 3682 (1966); R. L. Schwoebel, J. Appl. Phys. **40**, 614 (1969).
[3] G. Ehrlich and F. G. Hudda, J. Chem. Phys. **44**, 1039 (1966).
[4] (a) R. Kunkel, B. Poelsema, L. K. Verheij, and G. Comsa, Phys. Rev. Lett. **65**, 632 (1990); (b) S. Esch, M. Hohage, T. Michely, and G. Comsa, Phys. Rev. Lett. **72**, 518 (1994).
[5] H. A. van der Vegt, H. M. van Pinxteren, M. Lohmeier, E. Vlieg, and J. M. C. Thornton, Phys. Rev. Lett. **68**, 3335 (1992).
[6] G. Rosenfeld, R. Servanty, Ch. Teichert, B. Poelsema, and G. Comsa, Phys. Rev. Lett. **71**, 895 (1993).
[7] J. Tersoff, A. W. Denier van der Gon, and R. M. Tromp, Phys. Rev. Lett. **72**, 266 (1994).
[8] J. Vrijmoeth, H. A. van der Vegt, J. A. Meyer, E. Vlieg, and R. J. Behm, Phys. Rev. Lett. **72**, 3843 (1994).
[9] G. Ehrlich, Surf. Sci. **246**, 1 (1991).
[10] G. Kellog, Surf Sci. Rep. **21**, 1 (1994).
[11] D. W. Bassett, Surf. Sci. **53**, 74 (1975).
[12] S.-C. Wang and T. T. Tsong, Surf. Sci. **121**, 85 (1982).
[13] H. Röder, E. Hahn, H. Brune, J. P. Bucher, and K. Kern, Nature (London) **366**, 141 (1993).
[14] H. Brune, H. Röder, Ch. Romainczyk, and K. Kern, Appl. Phys. A **60**, 167 (1995).
[15] Ch. Romainczyk, thèse, EPF Lausanne [Instr. Report No. 1289, 1994].
[16] Y. Li and A. DePristo, Surf. Sci. **319**, 141 (1994).
[17] H. Brune, H. Röder, C. Boragno, and K. Kern, Phys. Rev. Lett. **73**, 1955 (1994); H. Brune, K. Bromann, H. Röder, K. Kern, J. Jacobsen, K. Jacobsen, P. Stoltze, and J. Nørskov (to be published).
[18] R. Stumpf and M. Scheffler, Phys. Rev. Lett. **72**, 254 (1994).
[19] M. Villarba and H. Jonsson, Surf. Sci. **317**, 15 (1994).
[20] J. Jacobsen, K. Jacobsen, P. Stoltze, and J. Nørskov, Phys. Rev. Lett. **74**, 2295 (1995).
[21] S.-C. Wang and G. Ehrlich, Phys. Rev. Lett. **67**, 2509 (1991).
[22] J. A. Meyer, J. Vrijmoeth, H. A. van der Vegt, E. Vlieg, and R. J. Behm (to be published).
[23] H. Brune, H. Röder, C. Boragno, and K. Kern, Phys. Rev. B **49**, 2997 (1994).
[24] Th. Härtel, U. Strüber, and J. Küppers, Thin Solid Films **229**, 163 (1993).
[25] F. Sette, T. Hashizume, F. Comin, A. A. MacDowell, and P. H. Citrin, Phys. Rev. Lett. **61**, 1384 (1988).